Published in final edited form as:
Austin J Biomed Eng. 2014 March 5; 1(1): .

Comparison of Kinetic Models for Dual-Tracer Receptor Concentration Imaging in Tumors

Nazanin Hamzei[1], **Kimberley S Samkoe**[2,3], **Jonathan T Elliott**[2], **Robert W Holt**[2], **Jason R Gunn**[2], **Tayyaba Hasan**[4], **Brian W Pogue**[2,3,4], and **Kenneth M Tichauer**[1,*]

[1]Biomedical Engineering Despartment, Illinois Institute of Technology, Chicago IL 60616, USA

[2]Thayer School of Engineering, Dartmouth College, Hanover NH 03755, USA

[3]Department of Surgery, Dartmouth Medical School, Hanover NH 03755, USA

[4]Wellman Center for Photo medicine, Massachusetts General Hospital, Boston MA 02114, USA

Abstract

Molecular differences between cancerous and healthy tissue have become key targets for novel therapeutics specific to tumor receptors. However, cancer cell receptor expression can vary within and amongst different tumors, making strategies that can quantify receptor concentration *in vivo* critical for the progression of targeted therapies. Recently a dual-tracer imaging approach capable of providing quantitative measures of receptor concentration *in vivo* was developed. It relies on the simultaneous injection and imaging of receptor-targeted tracer and an untargeted tracer (to account for non-specific uptake of the targeted tracer). Early implementations of this approach have been structured on existing "reference tissue" imaging methods that have not been optimized for or validated in dual-tracer imaging. Using simulations and mouse tumor model experimental data, the salient findings in this study were that all widely used reference tissue kinetic models can be used for dual-tracer imaging, with the linearized simplified reference tissue model offering a good balance of accuracy and computational efficiency. Moreover, an alternate version of the full two-compartment reference tissue model can be employed accurately by assuming that the K_1s of the targeted and untargeted tracers are similar to avoid assuming an instantaneous equilibrium between bound and free states (made by all other models).

Introduction

In cancer research, 95% of new therapeutics fail to demonstrate significant outcomes in clinical trials and are therefore abandoned after substantial investment [1,2], even though many of these therapeutics are designed to target cancer-specific receptors, being the products of highly sophisticated studies in cancer molecular expression [3]. While there is no consensus as to why so many drugs are failing clinical trials, it is clear that drug developers require new non-invasive methods to quantify cancer receptor concentrations *in vivo* in order to better understand the relationship between receptor availability, and drug

[*]**Corresponding author:** Biomedical Engineering, Illinois Institute of Technology, 3255 S Dearborn St, Chicago, IL, 60616, USA, tichauer@iit.edu.

targeting and binding [4]. Unfortunately, it has been difficult to extract quantitative information about tumor receptor concentrations with conventional molecular imaging strategies. They typically involve injecting a subject with an imaging tracer targeted to a receptor of interest, waiting some duration of time for any unbound tracer to exit the tissues, and assuming the remaining measured signal arises from tracer that is bound to its specific receptor. The problem is that drug delivery research in oncology has demonstrated that many physiological and path physiological factors (*e.g.*, blood flow, vascular permeability, interstitial pressure, and lymphatic drainage) can significantly influence the uptake of a targeted tracer in a tumor [5-8].

In response, “dual-tracer” imaging utilizes the uptake of a second tracer, similar to the targeted tracer but designed to be untargeted, to account for any non-receptor mediated uptake of the targeted tracer [9,10]. This approach was recently advanced by the development and validation of the first imaging methodology capable of quantifying receptor concentrations tumors [11]. The importance of using this “dual-tracer” approach over “reference tissue” approaches - which have been used for over a decade in brain studies to quantify neurotransmitter receptor concentrations [12] – was also demonstrated to be critical when attempting to quantify receptor concentration in tumors [13].

To date, the dual-tracer receptor concentration imaging (RCI) approaches have rather indiscriminately employed one of the two early reference tissue models, Lammertsma and Hume’s “simplified reference tissue model” [14] and Logan et al.’s “graphical analysis” approach [15], for no other reason than that they were easily adaptable to the dual-tracer framework. Even though many of the assumptions made in reference tissue models hold for dual-tracer RCI, it is not necessary that these models are optimal since additional assumptions can be made with dual-tracer RCI: *e.g.*, that the delivery rates (K_1) of both tracers are the same if the chemical properties of the tracers are similar. Using both simulated and experimental data, the current study was carried out to identify the optimal data analysis workflow for translating targeted and untargeted tracer uptake curves in tumors to receptor concentration images, with particular emphasis on noise characteristics and computational cost of kinetic model data fitting.

Theory

Compartment models for dual-tracer kinetic analyses

Reference tissue compartment models are ideally suited for dual-tracer RCI since the setup of the dual-tracer compartment model (Figure 1) is nearly identical to that of the reference tissue model [14]. Both models recognize that non-specific uptake of a targeted tracer can significantly affect the relationship between tracer uptake and tracer binding or receptor concentration. The reference tissue model accounts for binding by employing the temporal uptake of the targeted tracer in a region devoid of targeted receptor (reference tissue) to account for non-specific uptake; while the dual-tracer approach employs the uptake of a second tracer, similar in structure to the targeted tracer but untargeted, in the same tissue as the targeted tracer to account for non-specific uptake. On the surface it would seem that whatever kinetic model was best for one approach would also be best for the other, but there

are subtle differences between the approaches that can impact the choice of the optimal kinetic model:

1. The plasma input function, C_p: in the reference tissue model, the reference input and the region-of-interest input intrinsically have the same plasma input function, so this is not a concern; however, in the dual-tracer model, both tracers used must have the same plasma kinetics of the course of imaging.
2. K_1/k_2 equivalency: in reference tissue models, it is assumed that the ratio of the tracer's extravasations and tissue-efflux rates, K_1 and k_2, are equivalent in the reference tissue and the region of interest; whereas, dual-tracer models assumes that these leakage kinetics are the same between tracers in all tissues.

In this study, six different reference tissue models are evaluated in terms of their ability to accurately and efficiently estimate tumor cell-surface receptor concentration from dual-tracer data. The models included **1)** the "full reference tissue model" [FRTM] [16,17], later modified to a "reduced full reference tissue model" [Reduced FRTM] **2)** the "simplified reference tissue model" [SRTM] [14], **3)** The original graphical analysis reference tissue model [GARTM] [15], **4)** A linearized version of the SRTM [SRTM_lin] [18], **5)** A modification to the GARTM [GARTM_mod] [19], and **6)** the "basis function method" [BFM] [20]. While a full derivation of these six models is outside of the scope of this article, a presentation of the key mathematical expressions converted to a dual-tracer nomenclature are provided below. The FRTM can be expressed as:

$$\begin{aligned} ROI_T(t) &= R_1\left[ROI_U(t) + a\cdot ROI_U(t) * e^{-ct} + b\cdot ROI_U(t) * e^{-dt}\right], \\ with\quad & a = (k_3 + k_4 - c)\cdot(c-r)/p \\ & b = (d - k_3 - k_4)\cdot(d-r)/p \\ & c = (s+p)/2 \\ & d = (s-p)/2 \\ & p = \sqrt{s^2 - q} \\ & q = 4k_2k_4 \\ & r = k_2/R_1 \\ & s = k_2 + k_3 + k_4 \\ & * = \text{convolution integral}, \end{aligned} \tag{1}$$

where $ROI_T(t)$ and $ROI_U(t)$ represent the measured uptake curves of the targeted and untargeted tracers, respectively, in any region of interest, as a function of time, t; R_1 is the ratio of the rates of extravasation (K_1) of the targeted tracer and the untargeted tracer; k_2 is the rate of efflux of the targeted tracer; and k_3 and k_4 are the rates of association and dissociation of the targeted tracer, respectively (Figure 1).

Likewise, the SRTM can be expressed as:

$$ROI_T(t) = R_1\cdot ROI_U(t) + k_2\left(1 - \frac{R_1}{1+BP}\right) ROI_U(t) * e^{-\frac{k_2}{1+BP}t} \tag{2}$$

where BP, the “binding potential”, is equivalent to k_3/k_4, and is a key parameter since it represents the product of the receptor concentration (the parameter of interest) and the affinity of the targeted tracer for its receptor (which can in most cases be measured *ex vivo*) [12]. Going on, the format of the GARTM can be represented by:

$$\frac{\int_0^t ROI_T(u)\,du}{ROI_T(t)} = (1+BP)\,\frac{\int_0^t ROI_U(u)\,du + {}^{ROI_U(t)}/_{k_2}}{ROI_T(t)} + int, \quad (3)$$

where *u* is a dummy time variable to integrate over, int is an often neglected intercept term in this linear relationship with slope 1+*BP* at time, t > t*, where t* represents the time it takes for the C_f and C_b to reach a constant ratio (quasi-equilibrium). The format of the SRTM_lin can be expressed as follows:

$$ROI_T(t) = \left[R_1 \cdot ROI_U(t) + k_2 \int_0^t ROI_U(u)\,du\right] - \left(\frac{k_2}{1+BP}\right)\int_0^t ROI_T(u)\,du. \quad (4)$$

Furthermore, the format of the GARTM_mod can be expressed as follows:

$$\frac{\int_0^t ROI_T(u)\,du}{ROI_U(t)} = (1+BP)\,\frac{\int_0^t ROI_U(u)\,du}{ROI_U(t)} + int', \quad (5)$$

Where int’ represents another neglected intercept that is different in composition than the one in Eq. (3).

Finally, Gunn’s basis function method (BFM) is derived from Eq. (2) and is formulated as:

$$ROI_T(t) = \theta_1 ROI_U(t) + \theta_2 B_i(t) \quad (6)$$

Where $\theta_1 = R_1$, $\theta_2 = k_2 - R_1 k_2/(1+BP)$, B_i’s are he so-called basis functions defined as:

$$B_i(t) = ROI_U(t) \otimes e^{-\theta_{3,i}t} \quad (7)$$

And $\boldsymbol{q_3 = k_2 / (1+ BP)}$**;** so that Eq. (6) can be optimized for θ_1 and θ_2 in a linear least squares sense; provided that θ_3 is varied iteratively over a specified range.

Materials and Methods

Animal experiments

Targeted and untargeted tracer uptake curves were measured in two different tumor lines grown subcutaneously in athymic mice (*n* = 10, Charles River, Wilmington, MA). The targeted tracer was a ligand for the epidermal growth factor receptor (EGFR), a receptor that is over expressed in many cancers [21]. Specifically, the tracer was a near-infrared

fluorescent molecule bound to native epidermal growth factor, IRDye-800CW-EGF (LI-COR Biosciences, Lincoln, NE). The untargeted tracer was a free near-infrared fluorescent tracer emitting fluorescence at a separate wavelength, IRDye-700 (LI-COR Biosciences). The two different tumor lines were selected so as to represent different levels of epidermal growth factor receptor (EGFR) and were each implanted into six of the twelve immune-deficient mice (Charles River, Wilmington, MA). Five mice were inoculated with a human neuronal glioblastoma (U251; supplied from Dr. Mark Israel, Norris Cotton Cancer Center, Dartmouth-Hitchcock Medical Center), a cancer cell line known to express moderate levels of EGFR [22,23]; and another five mice were inoculated with a human epidermoid carcinoma (A431; ATCC, Manassas, VA), known to express a very large amount of EGFR [24]. In all cases, the tumors were introduced by injecting 1×10^6 tumor cells in Matrigel® (BD Biosciences, San Jose, CA) into the subcutaneous space on the left thigh of the mice. The tumors were then allowed to grow to a size of approximately 150 mm^3 before imaging.

The mice were anesthetized with ketamine-xylazine (100 mg/kg: 10 mg/kg *i.p.*) and the superficial tissue surrounding the tumors was removed. Each mouse was then placed tumor-side down on a glass slide and loosely secured with surgical tape (Figure 1). Once plated, the mice were positioned onto the imaging plane of an Odyssey Scanner (LI-COR Biosciences, Lincoln, NE). The Odyssey Scanner employs raster scanning and two lasers (one emitting at 685 nm and another at 785 nm) to excite two fluorophores simultaneously, pixel-by-pixel, and utilizes a series of dichroic mirrors to decouple fluorescence from the LI-COR 680 or 700 nm fluorescent tracers and the LI-COR 800 nm fluorescent tracer, respectively. All mice were injected with a cocktail of 1 nanomole of an EGFR targeted fluorescent tracer and 1 nanomole of an untargeted fluorescent tracer: the untargeted tracer was a carboxylate form of the IRDye 700DX NHS Ester (LI-COR Biosciences, Lincoln, NE) and the targeted tracer was IRDye 800CW-EGF (LI-COR Biosciences, Lincoln, NE). The mice were then imaged at approximately 3-min intervals for 1 h after injection of the fluorescent tracers.

Image analysis

The first step in the image analysis was to remove auto fluorescence (background fluorescence from the datasets. This was done by subtracting a pre-injection image of targeted and untargeted tracer channel fluorescence from all subsequent post-injection images [25]. Next, the potential differences in detection efficiency at the two wavelengths were normalized by taking the ratio of measured fluorescence from the targeted and untargeted tracers in a region of interest devoid of targeted receptor, and multiplying this "normalization" factor with all uptake images [11]. A pixel-wise fitting procedure was then performed according to each of the six aforementioned models in the tumor and surrounding tissues to calculate parametric maps of binding potential (which for the targeted tracer employed, is equivalent to EGFR concentration in units of nM because the affinity of EGF for EGFR is 1 nM^{-1} [26] and receptor concentration is equivalent to the product of the binding potential and the tracer affinity [12]). In the case of the FRTM, SRTM, and SRTM_lin models, their use was additionally tested when holding the parameter $R_1 = 1$, since it is the ratio of K_1s of the targeted and untargeted tracers, which should be equivalent [13]. MATLAB (Natick, MA) was used for all curve fitting procedures and the built in

function *lsqcurvfit()* was used for non-linear fitting (FRTM & SRTM), while *polyfit()* was used for the GARTM and GARTM_mod models, and the back-slash operator was used for SRTM_lin model. For the BFM model, the simulation was performed using both the conventional QR decomposition approach [20] and the back-slash operator. All curves were interpolated to 0.1 min temporal resolution using *interp1()* with a spline approach prior to the use of convolution or integration algorithms in MATLAB to avoid discretization errors.

Simulated data

As an initial test of the six models described in the Theory, targeted and untargeted tracer uptake curves were simulated for a typical level of EGFR expression in a moderate expressing tumor (2 nM [11]). The targeted tracer uptake curve was simulated based on a full solution to the two-tissue compartment model depicted in Figure 1 - that can be found in Appendix A of Lammertsma *et al*. [17] and the untargeted tracer uptake curve was simulated based on a one-tissue compartment model, also known as the Kety model [27]. Each of these model-types requires a plasma input function, *i.e.*, the concentration of the tracer in the blood over time, which was chosen from blood sampling experiments published previously [28] that were carried out in a cohort of 13 mice using the same targeted and untargeted tracers used in the current study. Furthermore, the rate constants K_1-k_4 needed to be assumed. For the purposes of the simulations here we assumed that the untargeted tracer was an ideal pair for the targeted tracer and therefore K_1 and k_2 were assumed to be equivalent between the tracers. Values of K_1 and k_2 were chosen based on the work of de Lussanet *et al*. who evaluated these parameters in tumors for different sized contrast agents; values associated with the 3.0-kDa agent were chosen as it most closely matched the size of the targeted tracer employed in the animal experiments (~ 7 kDa): the values were $K_1 = 0.013$ min^{-1} and $k_2 = 0.13$ min^{-1}[29]. The disassociation binding rate constant k_4 is equivalent to k_{off} in enzyme kinetic nomenclature and was measured by Zhou *et al*. to be approximately 0.1 min^{-1} for EGF bound to EGFR [26] - native EGF was the targeting moiety used in the animal experiments in this study. Then with binding potentials (k_3/k_4) roughly equivalent to 2 for a typical EGFR over expressing tumor line (U251: see *Animal experiments*), k_3 was by association assumed to be equal to 0.2 min^{-1}. The binding rates would be equivalent to a 2 nM concentration of EGFR using a native EGF based targeted tracer. All simulated targeted and untargeted tracer uptake curves were interpolated to 1-minute interval time-points from 1 to 60 min after tracer injection.

To best represent the actual animal data, a pixel-wise noise detection technique was performed to approximate the noise variance (percentage) in the Odyssey Scanner images. At each pixel, the targeted and untargeted uptake curves at all time points were extracted and fitted to a fifth-order polynomial (Figure 1d). The standard deviation of the error between the fit and the actual curves was averaged over all pixels in a region of interest and normalized by the maximum value of the curves to represent an overall measure of noise in that region. It was noticed that the noise metric was generally less in the untargeted uptake curves compared to the targeted ones but, without loss of generality, this fact was not incorporated in the simulations. In most cases (for different images and different regions of interest), the average noise did not exceed 3% of the signal; therefore, 3% Gaussian noise

was added to all simulated tracer uptake curves prior to employing the kinetic models described in the Theory to back-out the simulated EGFR concentration.

Results and Discussion

Figure 2 presents the average EGFR concentrations measured using all models described in the Theory. All of the models produced very similar results with the spread in averages being about 25% of the mean. There were no statistically significant differences between the results of any of the models except for the GARTM_mod, which produced significantly lower estimates of EGFR than all other models in both tumor groups ($n = 5$ in each tumor group, $p < 0.05$).

Figure 3 presents parametric maps from one typical U251 mouse and one A431 mouse for each of the tested kinetic models. On the whole, the visual quality (in terms of pixel fitting robustness to noise) of the parametric maps was adequate and comparable between models. Only the SRTM_lin model appeared to suffer from some instability. Upon noise analysis (Figure 4), it did not appear than the instability in EGFR concentration estimation of the SRTM_lin resulted from a heightened sensitivity to noise. Rather, it appears as if the model becomes unstable in tissues with very little targeted tracer binding. The current implementation of SRTM_lin in this paper utilizes a “back-slash” operation in MATLAB; however, future applications could include iterative fitting routines that would slow the algorithm down, but would allow constraints to be enacted that could improve the stability.

There are no quantitative gold standard methods for measuring *in vivo* receptor concentrations, so it is difficult to determine whether the GARTM_mod of the other models were more accurate from the experimental data alone. In a separate study, *ex-vivo*rough estimates of EGFR concentration in the U251 tumors and A431 tumors were 1.6 ± 0.4 and 2.7 ± 0.4 nM, respectively [11], suggesting perhaps that the GARTM_mod would be most accurate, but the rough estimates should not be held as quantitative and therefore cannot be used to make any conclusions other than supporting the fact that the A431 expresses significantly more EGFR than the U251 tumors (a trend strongly supported by all models). In response, a number of simulation studies were carried out to better evaluate the accuracy and precision of the various approaches.

Figures 4 and 5 present the results of the simulation studies described in the Methods, with numerical results of accuracy, precision, and computational cost, summarized in Table 1. The SRTM, SRTM_lin, and reduced FRTM results all provided the most accurate results, with the BFM and GARTM slightly underestimating the simulated level of receptor concentration, and the GARTM_mod, strongly underestimating the simulated receptor concentration. The fact that GARTM_mod does not work for our case was expected, since according to the authors of the approach, it has been developed for the special case of PET imaging in rats and is not guaranteed to work in other frameworks [19]. Interestingly though, in a comparative sense, the GARTM_mod appeared to be fair much better in the animal experiments than in simulations, and could be considered a viable model owing to its computational efficiency and the fact that it does not require an estimate of k_2 like the GARTM.

With respect to the GARTM, the slight underestimation in receptor concentration estimation is a well-known phenomenon of the model attributable to a noise bias [30]; however, it should be noted that novel adaptations of the GARTM have been developed to account for this noise bias [31]. The fact that such an underestimation was not observed in the animal experiments compared to the SRTM based models could have stemmed from an overestimation in the assumed value of k_2 (which was assumed to be 0.1 min^{-1} in the animal experiments). Figure 6 presents a sensitivity profile of the error in receptor concentration estimation using GARTM given errors in assumed k_2 for tracers of different sizes from small to x-large, using K_1 and k_2 parameters from de Lussanet et al. As a reference [29]. The slight underestimation in receptor concentration of the BFM was found to be attributable to the fit constraints, which are effectively realized in the pre-specified range for θ_3.In fact, the BFM could perhaps be considered the best overall model if it weren't for the known sensitivity in estimations to the parameters of the fit [20]. The model is nearly as fast as SRTM_lin, more stable in low binding tissues, and can have excellent accuracy and precision; although its sensitivity to the constraints, especially to the lower bound of the θ range, is such that a 1 percent change in the lower bound could sometimes yield a 20 percent change in the estimated BP value.

All figures do not include results from the FRTM because fits using this model resulted in largely spurious estimates of EGFR concentration estimates of −0.03 and −0.05 for the U251 and A431 tumor groups, respectively. It may just be that the model requires careful consideration of starting parameters and constraints in the fitting; however, the fourth degree of freedom is known to be problematic, which is why this model is rarely used in reference tissue modelling [14].The "reduced" FRTM, however, wherein R_1 was set equal to 1 to reduce the number of fitting parameters to three (a constraint only possible in dual-tracer imaging and not possible in reference tissue modelling), produced promising results. According to this finding, it was presumed that a similar constraint (setting R_1=1) would also improve the characteristics of the SRTM and SRTM_lin; however, these new "two-parameter" models were tested both in simulation and on the animal data, where they were found to be very unstable. Presumably, this is because including R_1 as a fitting parameter provides a necessary degree of freedom to deal with small differences in scale between the targeted and untargeted tracer uptake curves that was unnecessary in the reduced FRTM (i.e., fitting for R_1 can help account for any bias caused by noise or imprecise detector efficiency normalization, while setting it to 1 causes other parameters to suffer from the bias in a more unstable manner).

One very interesting potential advantage of the reduced-FRTM that requires future study, is that it is the only model that does not make an assumption of an instantaneous equilibrium between the free and bound concentrations of targeted tracer in its compartment model (the so-called "adiabatic approximation" [14]) (Figure 1c). The binding kinetics of EGF [26], the targeting ligand employed in the animal experiments in this study, and the similar levels of k_3 and k_4 employed in the simulations, appear to support the adiabatic approximation; however, larger, more specific targeting moieties may have slower binding kinetics that would preclude validity of the approximation [32]. It is for these applications that the reduced-FRTM could have a unique advantage.

Some other less substantial findings warrant some discussion. It was found that the specification of upper and lower bounds for models using the built-in function *lsqcurvefit()* was an issue that needed to be dealt with carefully. Without specifying the proper bounds, SRTM and the Reduced FRTM tended to produce out of bound or 'saturated' values for EGFR concentration at some pixels in the animal experiment results (presumably owing to noise and the abnormal behaviour of the targeted and untargeted curves at those pixels). Cselenyi et al [33]. Have set these outlier values to zero in their algorithm, thus getting binding potential maps that contain 'holes'[33].In this study, the fitting procedure was constrained instead, by manually altering the constraints until achieving the optimum results and a 'clean' parametric map. Future work is ongoing to determine a more automated approach for selecting the parameters of the fit.

In terms of speed, the SRTM_lin model was the fastest and the Reduced FRTM the slowest. SRTM was about 10 times slower than GARTM and BFM, but not necessarily more efficient. For SRTM and Reduced FRTM, MATLAB's *lsqcurvefit()* function was used to incorporate constraints on fitted values; otherwise the models would overload for some experimental cases. The employment of *lsqcurvefit()* in these models had two effects: first, it slowed down the optimization algorithm (SRTM_lin is the fastest because it does not use such constraints and performs the fit with a simple back-slash operator); second, the constraints need to be manually selected for each case to avoid out of bound values for fit parameters. It would be worthwhile to employ other optimization toolboxes for these two models to both speed them up and also automate the process of finding their constraints. The Reduced FRTM could also be linearized in a similar manner as SRTM_lin for increased speed. This is left for future studies.

Conclusion

A reduced version of the full two-compartment kinetic model, along with five other prevalent kinetic modelling approaches used widely in tracer kinetics nomenclature were studied, implemented, and evaluated in this study; with particular emphasis on employment of these models in a dual-tracer modelling framework. Evaluation was carried out in EGFR targeted studies in experimental mouse tumor xenograft models, and was supported by theoretical simulations. In general, no single model outperformed the others for dual-tracer modelling; instead, each model came with their own strengths and weaknesses. Overall, the reduced FRTM, SRTM, and SRTM_lin models provided the most accurate estimates of binding potential in simulations and experimental results; however, they did result in larger variation to noise compared to GARTM and the Gunn approaches. One potential advantage of the reduced FRTM is that it is the only model that does not assume an instantaneous equilibrium between the bound and free compartments of the targeted tracer model. Future work will explore the potential advantages of this model for estimating binding kinetics of larger targeting moieties such as antibodies that may not obey this assumption [32]. If the instantaneous equilibrium assumption is valid, the SRTM_lin model could be argued to provide a good balance of advantages. It was cosnsiderably faster than all other models except for GARTM, it does not require an estimate of k_2 (as is the case with GARTM), and it provided the most accurate results in simulations.

Acknowledgments

This research was funded by NIH grants P01CA84201, R01CA156177, and U54CA151662. K M T and J T E acknowledge funding from the CIHR postdoctoral fellowship program. We would also like to thank Kristian J Sexton and Harold H. Yang for their assistance with running the animal experiments.

References

1. Arrowsmith J. Trial watch: Phase II failures: 2008-2010. Nat Rev Drug Discov. 2011; 10:328–329. [PubMed: 21532551]
2. Arrowsmith J. Trial watch: phase III and submission failures: 2007-2010. Nat Rev Drug Discov. 2011; 10:87. [PubMed: 21283095]
3. Sawyers C. Targeted cancer therapy. Nature. 2004; 432:294–297. [PubMed: 15549090]
4. Weissleder R, Pittet MJ. Imaging in the era of molecular oncology. Nature. 2008; 452:580–589. [PubMed: 18385732]
5. Jain RK. Physiological barriers to delivery of monoclonal antibodies and other macromolecules in tumors. Cancer Res. 1990; 50:814s–819s. [PubMed: 2404582]
6. Jain RK. Vascular and interstitial barriers to delivery of therapeutic agents in tumors. Cancer Metastasis Rev. 1990; 9:253–266. [PubMed: 2292138]
7. Maeda H, Wu J, Sawa T, Hori K, Matsumura Y. Tumor vascular permeability and the EPR effect in macromolecular therapeutics: a review. J Control Release. 2000; 65:271–284. [PubMed: 10699287]
8. Wang D, Chen Y, Liu JT, Leigh SY, Contag CH, et al. Microscopic Delineation of Medulloblastoma Margins in a Transgenic Mouse Model Using a Topically Applied VEGFR-1 Probe. Transl Oncol. 2012; 5:408–414. [PubMed: 23323155]
9. Pogue, Brian W.; Samkoe, Kimberley S.; Hextrum, Shannon; O'Hara, Julia A.; Jermyn, Michael, et al. Imaging targeted-agent binding in vivo with two probes. J Biomed Opt. 2010; 15:030513. [PubMed: 20614996]
10. Liu JT, Helms Mike W, Mandella Michael J, Crawford James M, Kino Gordon S, et al. Quantifying cell-surface biomarker expression in thick tissues with ratiometric three-dimensional microscopy. Biophys J. 2009; 96:2405–2414. [PubMed: 19289065]
11. Tichauer KM, Samkoe Kimberley S, Sexton Kristian J, Hextrum Shannon K, Yang Harold H, et al. In vivo quantification of tumor receptor binding potential with dual-reporter molecular imaging. Mol Imaging Biol. 2012; 14:584–592. [PubMed: 22203241]
12. Innis RB, Votaw John R, Wong Dean F, Sossi Vesna, Mintun A, et al. Consensus nomenclature for in vivo imaging of reversibly binding radioligands. J Cereb Blood Flow Metab. 2007; 27:1533–1539. [PubMed: 17519979]
13. Tichauer KM, Samkoe KS, Klubben WS, Hasan T, Pogue BW, et al. Advantages of a dual-tracer model over reference tissue models for binding potential measurement in tumors. Phys Med Biol. 2012; 57:6647–6659. [PubMed: 23022732]
14. Lammertsma AA, Hume SP. Simplified reference tissue model for PET receptor studies. Neuroimage. 1996; 4:153–158. [PubMed: 9345505]
15. Logan J, Fowler Joanna S, Volkow Nora D, Wang Gene-Jack, Ding Yu-Shin, et al. Distribution volume ratios without blood sampling from graphical analysis of PET data. J Cereb Blood Flow Metab. 1996; 16:834–40. [PubMed: 8784228]
16. Hume SP, Myers Ralph, Bloomfield Peter M, Opacka-Juffry Jolanta, Cremer Jill E, et al. Quantitation of carbon-11-labeled raclopride in rat striatum using positron emission tomography. Synapse. 1992; 12:47–54. [PubMed: 1411963]
17. Lammertsma AA, Bench CJ, Hume SP, Osman S, Gunn K, et al. Comparison of methods for analysis of clinical [11C] raclopride studies. J Cereb Blood Flow Metab. 1996; 16:42–52. [PubMed: 8530554]
18. Masanori, Ichise; Toyama, Hiroshi; Innis, Robert B.; Carson, Richard E. Strategies to improve neuroreceptor parameter estimation by linear regression analysis. J Cereb Blood Flow Metab. 2002; 22:1271–1281. [PubMed: 12368666]

19. Topping GJ, Dinelle Katie, Kornelsen Rick, McCormick Siobhan, Holden James E, et al. Positron emission tomography kinetic modeling algorithms for small animal dopaminergic system imaging. Synapse. 2010; 64:200–208. [PubMed: 19862685]
20. Gunn RN, Lammertsma Adriaan A, Hume Susan P, Cunningham Vincent J. Parametric imaging of ligand-receptor binding in PET using a simplified reference region model. Neuroimage. 1997; 6:279–287. [PubMed: 9417971]
21. Nicholson RI, Gee JM, Harper ME. EGFR and cancer prognosis. Eur J Cancer. 2001; 37:S9–S15. [PubMed: 11597399]
22. Gibbs-Strauss SL, Samkoe Kimberley S, O'Hara Julia A, Davis Scott C, Jack Hoopes P, et al. Detecting epidermal growth factor receptor tumor activity in vivo during cetuximab therapy of murine gliomas. Academic radiology. 2010; 17:7–17. [PubMed: 19796971]
23. Smith JJ, Derynck R, Korc M. Production of transforming growth factor alpha in human pancreatic cancer cells: evidence for a superagonist autocrine cycle. Proceedings of the National Academy of Sciences of the United States of America. 1987; 84:7567–7570. [PubMed: 3499610]
24. Wikstrand, Carol J.; McLendon, Roger E.; Friedman, Allan H.; Bigner, Darell D. Cell surface localization and density of the tumor-associated variant of the epidermal growth factor receptor, EGFRvIII. Cancer research. 1997; 57:4130–4140. [PubMed: 9307304]
25. Samkoe KS, Kristian Sexton, Kenneth M, Tichauer, Shannon K, Hextrum, Omar Pardesi, et al. High vascular delivery of EGF, but low receptor binding rate is observed in AsPC-1 tumors as compared to normal pancreas. Mol Imaging Biol. 2012; 14:472–479. [PubMed: 21847690]
26. Zhou M, Felder S, Rubinstein M, Hurwitz DR, Ullrich A, et al. Real-time measurements of kinetics of EGF binding to soluble EGF receptor monomers and dimers support the dimerization model for receptor activation. Biochemistry. 1993; 32:8193–8198. [PubMed: 8347619]
27. Kety SS. The theory and applications of the exchange of inert gas at the lungs and tissues. Pharmacol Rev. 1951; 3:1–41. [PubMed: 14833874]
28. Tichauer KM, Samkoe Kimberley S, Sexton Kristian J, Gunn Jason R, Hasan Tayyaba, et al. Improved tumor contrast achieved by single time point dual-reporter fluorescence imaging. J Biomed Opt. 2012; 17:066001. [PubMed: 22734757]
29. de Lussanet QG, Langereis Sander, Beets-Tan Regina GH, van Genderen Marcel HP, Griffioen Arjan W, et al. Dynamic contrast-enhanced MR imaging kinetic parameters and molecular weight of dendritic contrast agents in tumor angiogenesis in mice. Radiology. 2005; 235:65–72. [PubMed: 15731376]
30. Logan J, Fowler Joanna S, Volkow Nora D, Ding Yu Shin, Wang Gene-Jack, et al. A strategy for removing the bias in the graphical analysis method. J Cereb Blood Flow Metab. 2001; 21:307–320. [PubMed: 11295885]
31. Logan J, Alexoff D, Fowler JS. The use of alternative forms of graphical analysis to balance bias and precision in PET images. J Cereb Blood Flow Metab. 2011; 31:535–546. [PubMed: 20808318]
32. Thurber GM, Dane Wittrup K. A mechanistic compartmental model for total antibody uptake in tumors. J Theor Biol. 2012; 314:57–68. [PubMed: 22974563]
33. Cselenyi Z, Olsson Hans, Halldin Christer, Gulyás Balázs, Farde Lars, et al. A comparison of recent parametric neuroreceptor mapping approaches based on measurements with the high affinity PET radioligands [11C]FLB 457 and [11C]WAY 100635. Neuroimage. 2006; 32:1690–1708. [PubMed: 16859930]

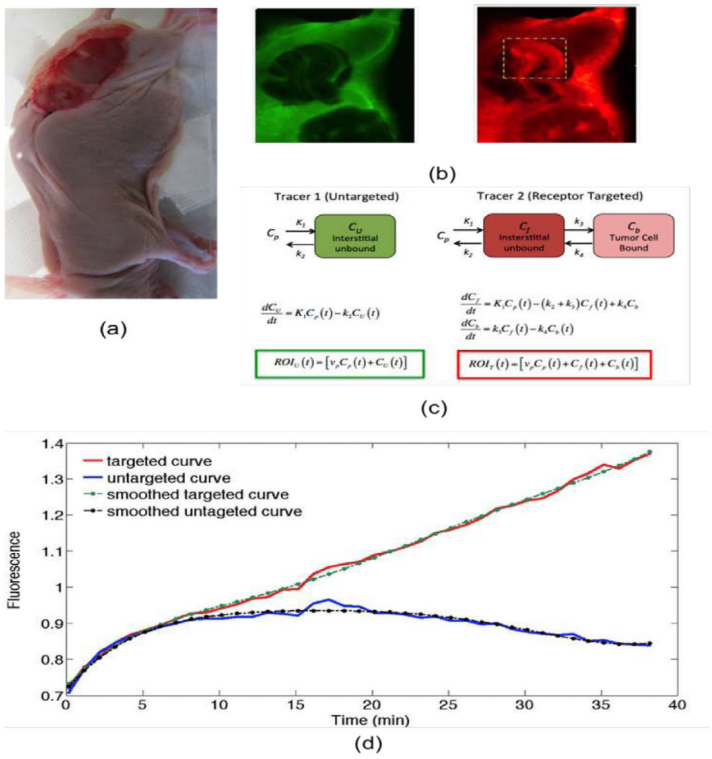

Figure 1.

A photograph of the dual-tracer experimental setup of a U251 mouse with tumor exposed is presented in (a): targeted tracer (red) and untargeted tracer (green) fluorescence uptake images at 60 min post-tracer injection are presented in (b). The tumor area has been marked by the dashed rectangle (b), and the corresponding compartment models (c). $ROI_T(t)$ and $ROI_U(t)$ represent the measured uptake curves of the targeted and untargeted tracers, respectively, in any region of interest, as a function of time, t; v_p is the blood volume percentage in the tumor; K_1 and k_2 are the rates of exchange of the tracers from the blood concentration (C_p) to the interstitial space (C_f for the targeted tracer and C_U for the untargeted tracer) and back, respectively; and k_3 and k_4 are the rates of association and dissociation of the targeted tracer to its receptor in a bound state (C_b). Typical uptake curves of the targeted tracer (red) and the untargeted tracer (blue) in a single pixel in a low signal-to-noise scenario is presented in (e). The smooth "fits" are polynomials fit to the data to determine the noise characteristics.

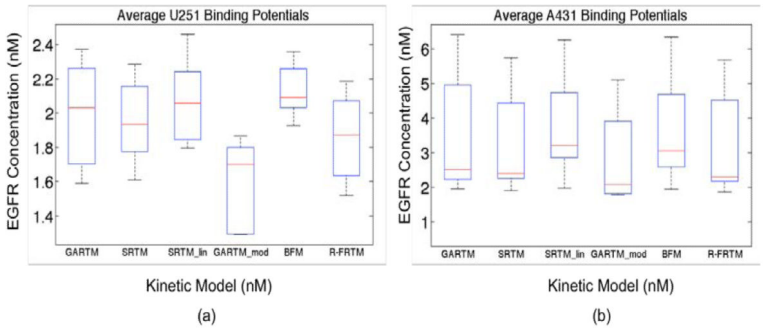

Figure 2.

Box plots of epidermal growth factor (EGFR) concentration estimates from all models are presented in (a) for the human glioma xenograft mice (U251 cell line) and in (b) for the human epidermoid xenograft mice (A431 cell line). The kinetic models are the graphical analysis reference tissue model (GARTM), the simplified reference tissue model (SRTM), the linearized-SRTM (SRTM_lin), a modified GARTM (GARTM_mod), a basis function model (BFM), and a “reduced” full reference tissue model (R-FRTM). The red lines represent the median EGFR concentration estimates.

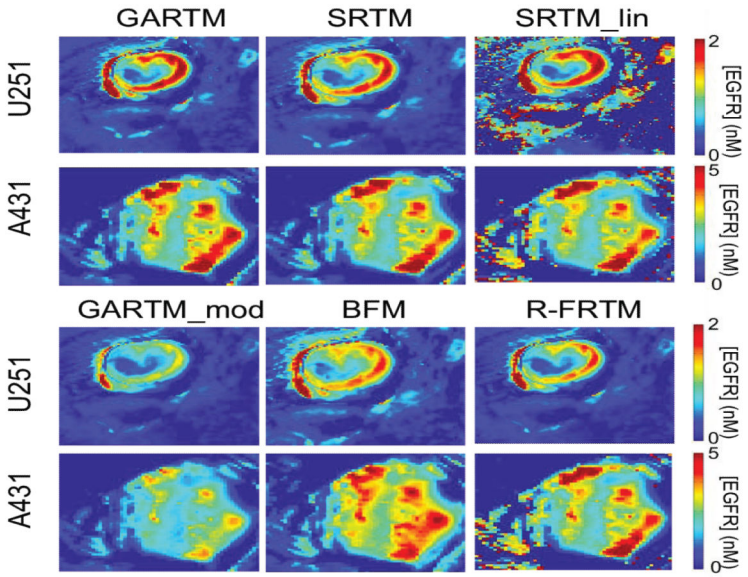

Figure 3.

Parametric maps of estimated epidermal growth factor receptor (EGFR) concentration. The SRTM_lin model lacks constraints and thus fails to produce maps as ‘clean’ as those generated by other models; as seen from the holes and saturated values in the maps on the top right of the figure.

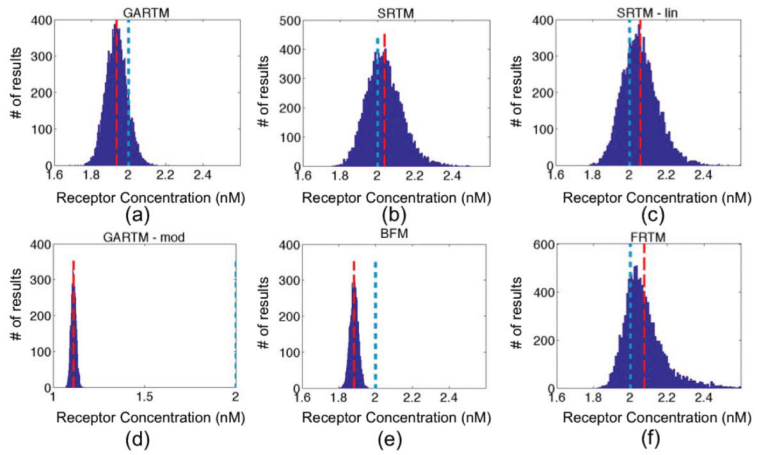

Figure 4.

Fitting receptor concentration results from applying the six models [graphical analysis reference tissue model (GARTM), the simplified reference tissue model (SRTM), the linearized-SRTM (SRTM_lin), a modified GARTM (GARTM_mod), a basis function model (BFM), and a "reduced" full reference tissue model (R-FRTM)] – (a)-(f), respectively – to simulated curves with additive Gaussian noise of 3% for 10,000 iterations. The red dashed and the blue dotted vertical lines indicate the positions of the means of the fit and the true BP respectively. The scales for horizontal axes are the same in all figures except GARTM_mod, which produced out of bound values for Binding Potential.

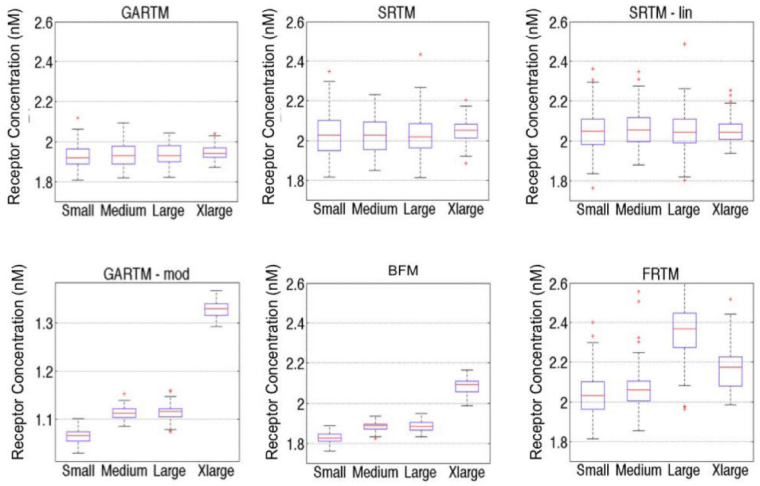

Figure 5.

Comparison of fitting performances of different models [graphical analysis reference tissue model (GARTM), the simplified reference tissue model (SRTM), the linearized-SRTM (SRTM_lin), a modified GARTM (GARTM_mod), a basis function model (BFM), and a "reduced" full reference tissue model (R-FRTM)] and different particles within each model. Fitting is done for 100 times for each particle within each model.

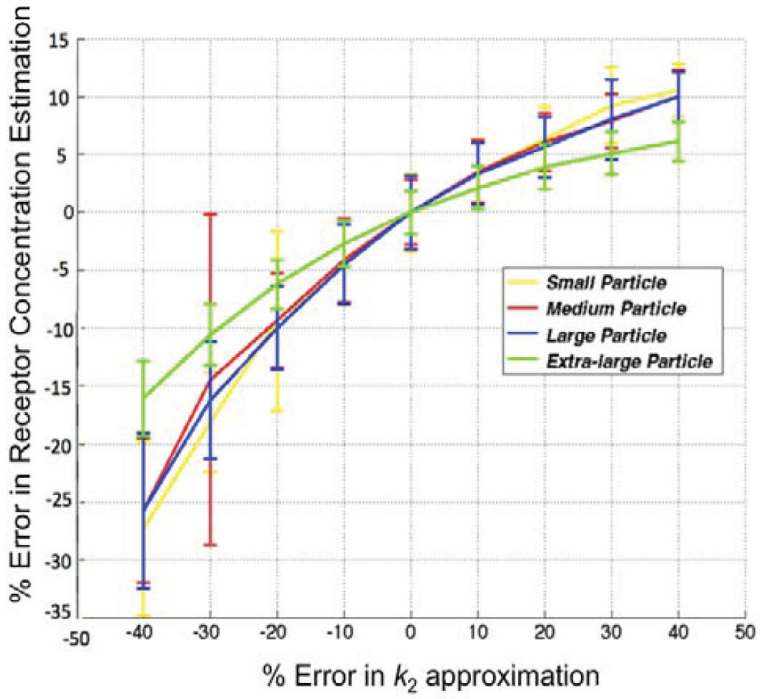

Figure 6.

Sensitivity of the results of the graphical analysis reference tissue model (GARTM) to errors in the value of k_2. The true k_2 is 0.13 in this case and the noise added to the curves is 3%.

Table 1

Comparison of the models in terms of accuracy and speed. The first and third rows show the means and standard deviation (sd) of the graphical analysis reference tissue model (GARTM), the simplified reference tissue model (SRTM), the linearized-SRTM (SRTM_lin), a modified GARTM (GARTM_mod), a basis function model (BFM), and a “reduced” full reference tissue model (R-FRTM) for the medium sized particle simulations. The fourth row represents the time taken for the models to perform the fit for 10000 iterations. These results and their interpretations may vary for different particles and computers.

	GARTM	**SRTM**	**SRTM_ lin**	**BFM**	**R-FRTM**	**GARTM_ mod**
Estimated Receptor Concentration (Mean ± SD)	1.9 ± 0.1	2.0 ± 0.1	2.1 ± 0.1	1.9 ± 0.0	2.1 ± 0.1	1.1 ± 0.0
Error in receptor concentration estimate	−0.06	0.04	0.06	−0.12	0.08	−0.89
Elapsed Time for 10,000 fits (s)	13	240	5	103	838	25